Wang *et al. J Mater Inf* 2024;4:29
DOI: 10.20517/jmi.2024.45

Journal of materials Informatics

Research Article

Open Access

Exploring phase transitions in CdSe: a machine learning and swarm intelligence approach

Meiyan Wang, Rishi Rao, Li Zhu*

Department of Physics, Rutgers University, Newark, NJ 07102, USA.

***Correspondence to:** Prof. Li Zhu, Department of Physics, Rutgers University, 101 Warren Street, Newark, NJ 07102, USA. E-mail: li.zhu@rutgers.edu

How to cite this article: Wang M, Rao R, Zhu L. Exploring phase transitions in CdSe: a machine learning and swarm intelligence approach. *J Mater Inf* 2024;4:29. http://dx.doi.org/10.20517/jmi.2024.45

Received: 8 Sep 2024 **First Decision:** 17 Oct 2024 **Revised:** 25 Nov 2024 **Accepted:** 28 Nov 2024 **Published:** 26 Dec 2024

Academic Editor: Xingjun Liu **Copy Editor:** Pei-Yun Wang **Production Editor:** Pei-Yun Wang

Abstract

The phase transition of cadmium selenide (CdSe) from wurtzite to rocksalt structure has been the subject of extensive research. In this study, we present a novel approach combining machine learning potentials with swarm intelligence-based pathway sampling to elucidate the complex phase transition mechanisms in CdSe. We developed an accurate machine-learning (ML) potential for CdSe, validated against density functional theory calculations, achieving mean absolute errors (MAEs) of 1.8 meV/atom for energies and 33 meV/Å for forces. This potential was integrated with the pathway sampling via swarm intelligence and graph theory (PALLAS) method to explore the potential energy landscape and identify low-energy transition pathways. Our simulations revealed a complex network of transition pathways, and we discovered a multi-step transition mechanism involving an unexpected zinc blende intermediate phase, which appears to play a crucial role in facilitating the transition between wurtzite and rocksalt structures. This finding provides new insights into the structural flexibility of CdSe and offers an explanation for experimentally observed phenomena such as wurtzite/zinc blende coexistence in nanostructures. Our approach not only advances the fundamental understanding of phase transitions in CdSe but also establishes a powerful computational framework for exploring complex materials phenomena, opening new avenues for materials design and discovery in semiconductor systems.

Keywords: Machine learning, phase transition, transition pathway prediction, CdSe, swarm intelligence

INTRODUCTION

Cadmium selenide (CdSe), a pivotal II-VI semiconductor material, has been the subject of extensive research due to its crucial applications in optoelectronics[1–3], photovoltaics[4–7], and nanostructured materials[8–11]. Its unique attributes, particularly at the nanoscale[8–11], have spurred a multitude of studies aimed at unraveling and leveraging its potential for advanced technological applications. Among the critical phenomena associated with CdSe, phase transitions, especially the transition from wurtzite to rocksalt structures, have garnered significant attention[11–27]. These transitions profoundly influence the electronic and optical properties, necessitating a comprehensive understanding at the atomic level to optimize the performance and efficiency of CdSe-based devices.

Significant progress has been made in understanding the phase transitions of CdSe across various scales and conditions. For example, Fan *et al.* demonstrated the ability to control the phase transition from the zinc blende to wurtzite phase in CdSe nanocrystals by varying the volume ratio of ethanolamine and water, providing valuable insights into the manipulation of phase and morphology in nanomaterials[20]. Durandurdu *et al.* observed a phase transition from the wurtzite to rocksalt structure in CdSe using constant-pressure *ab initio* molecular dynamics (MD) simulations, proposing a transformation mechanism involving orthorhombic intermediate phases[16]. Similarly, Li *et al.* investigated the structural phase transition sequence of CdSe under high pressure, offering critical insights into the material's behavior under extreme conditions[21]. Building on this foundation, Tolbert *et al.* explored the size-dependent phase transitions in CdSe nanocrystals, revealing how quantum confinement effects influence structural stability and phase behavior[22]. Their findings highlighted the pivotal role of surface energy and particle size in determining phase transition pressures, providing valuable guidance for tailoring the properties of CdSe nanostructures. More recently, *in situ* high-pressure synchrotron X-ray diffraction studies have elucidated the pressure-induced phase transitions in CdSe nanowires, demonstrating how nanostructuring influences transition pathways and mechanical properties[23]. A very recent study employed MD simulations with a machine-learning (ML)-based deep potential to uncover the crystallization mechanisms of CdSe, shedding light on the atomistic details of its structural transformations[27]. These advances collectively emphasize the diverse conditions and approaches that have been used to deepen our understanding of CdSe phase transitions, paving the way for further exploration of its structural dynamics. While much attention has been given to the effects of pressure and nanoscale features, a comprehensive understanding of the transition mechanisms in bulk CdSe remains critical. Bulk transitions provide a foundation for interpreting the behavior of nanostructures and offer insights into the intrinsic properties of the material. However, systematically sampling the phase transition pathway poses a challenging task due to the complexity and computational demands of accurately mapping the transition mechanisms. Methods such as the nudged elastic band (NEB) method[28,29] or transition path sampling (TPS)[30,31] have been employed to study phase transitions in materials, but these approaches often require an initial path connecting the reactant and product and may be computationally expensive for large systems. Standard MD simulations can provide insights into the dynamics of phase transitions, but they may limited by the time scales required to sample rare events.

In response to this challenge, we have recently developed the pathway sampling via swarm intelligence and graph theory (PALLAS) method[32], an innovative approach that combines swarm intelligence and graph theory. The method is adept at identifying low-energy transition pathways between two minima without the prerequisite of specifying the transition mechanism a priori. It underscores the effectiveness of combining swarm intelligence with computational strategies to elucidate phase transformations in solid-state systems. Builds upon previous work in swarm intelligence algorithms, such as particle swarm optimization (PSO)[33] and ant colony optimization[34], PALLAS adapts these techniques to the complex challenges of materials science.

Despite the ability of the PALLAS method in mapping transition pathways, the extensive sampling required is computationally burdensome, highlighting the need for a more efficient and accurate method of energy and force calculation. This computational challenge is not unique to our approach but is a common hurdle in ma-

terials simulation, as noted in the review of ML potentials for atomistic simulations[35]. In recent years, several studies have leveraged ML potentials to address this computational challenge and study phase transitions in semiconductors[27,36–41]. These studies demonstrate the growing capability of ML potentials to capture complex atomic interactions accurately while significantly reducing computational costs compared to traditional *ab initio* methods.

Our initial application of the PALLAS method used a force field approach[42] to discover new transition pathways for CdSe. However, while our previous study aimed to show the feasibility of the PALLAS method in exploring complex energy landscapes, it was limited by the accuracy of the employed force field[32]. This work addresses this need by applying a novel computational framework that combines ML-based potentials with the PALLAS methodology for transition pathway sampling. This approach enables the systematic exploration of phase transition pathways, uncovering insights into the structural transformations of CdSe at an unprecedented level of detail. Although our focus is on bulk transitions at ambient pressure and low temperatures, this work establishes a computational methodology that can be extended to address the effects of pressure and temperature as well as transitions in nanostructures. These extensions represent exciting avenues for future exploration, which we briefly discuss in the concluding sections.

METHODS

Transition pathway prediction

The transition pathway prediction method in this study is based on the recently developed PALLAS approach[32], which efficiently identifies low-energy transition pathways in solid-state systems without requiring predefinition of the mechanism. PALLAS integrates several key components: the solid-state dimer method for saddle point optimization[43]; a fingerprint method for quantifying structural dissimilarity[44]; multiobjective PSO for pathway optimization[45]; and graph theory for network analysis[46].

The PALLAS algorithm begins by generating random velocities for the reactant and product structures to displace them from their initial minima. The solid-state dimer method then locates saddle points and nearby minima from these configurations. A crystal fingerprint technique, based on Gaussian overlap matrices, measures configurational distances between structures, quantifying their similarity or dissimilarity. This approach captures both local atomic environments and global structural characteristics, allowing for an accurate representation of the configurational space[44,47–51]. The minima, transition states, and their connections form an undirected network graph. Graph algorithms, such as Kruskal's algorithm[52] and breadth-first search[53], analyze this network to identify optimal low-barrier transition routes. Multiobjective PSO guides the search by optimizing both the configurational distance and energy barriers along pathways, enabling efficient exploration of the potential energy surface (PES) for favorable transition mechanisms.

In the PALLAS method, several parameters remain fixed during the pathway sampling process to ensure consistency and reliability. The system composition and lattice parameters are kept constant, focusing exclusively on structural transformations without introducing compositional or volumetric changes. Additionally, in the multiobjective PSO, the learning factors c_1 and c_2 are set to 2, and the inertia weight ω is maintained within the range $0.4 \leq \omega \leq 0.9$, as this range is known to optimize performance. Random numbers r_1 and r_2 are independently generated within the range $(0, 1)$ for each iteration, ensuring dynamic but controlled updates to the particle positions. These fixed parameters provide stability and guide the efficient exploration of the PES.

This systematic approach allows PALLAS to identify the most energetically favorable transitions between crystalline phases without requiring prior knowledge of the mechanism. However, it is important to note that, similar to many computational methods, PALLAS has limitations. The identification of the global minimum

energy pathway is a non-deterministic polynomial-time (NP)-hard problem, and the algorithm relies on a practical halting criterion, terminating when no lower-energy pathway is found after ten consecutive generations. As a result, while PALLAS provides a comprehensive exploration of the energy landscape, it does not guarantee identification of the absolute global minimum barrier. Additionally, the current study does not incorporate entropy or temperature effects, which could influence transition pathways and metastable state stability.

PES modeling

To model the PES of CdSe accurately for our study on phase transition pathways, we employed the neural equivariant interatomic potentials (NequIP) framework[54]. NequIP represents a significant advancement in ML potentials, offering precise predictions of material properties through its innovative use of E(3)-equivariant neural networks. This approach is pivotal for simulating phase transitions by accurately predicting total energies and atomic forces while respecting the fundamental symmetries of the physical system.

Dataset generation

Our NequIP model was trained using an amalgamation of training data generated using different methods. A total of 1,750 structures were generated using an entropy maximization technique[55]. In short, this technique involves adding an entropy term to the total energy that is to be optimized. The entropy term comes from a descriptor, which we have chosen as a structural fingerprint descriptor[44]. The fingerprint descriptor provides a vector for every atom in the unit cell, with the Euclidean distance between two different atomic fingerprint vectors indicating the dis-similarity of their chemical environments. The entropy term is then calculated as

$$S(\{\mathbf{q}\}) = \frac{1}{n}\sum_{j=1}^{n} Ln(n \min_{l\neq j} \Delta q_{j,l}) \tag{1}$$

Where n is the number of atoms in the unit cell, $\{\mathbf{q}\}$ is the set of all fingerprint descriptor vectors for each atom in the unit cell, and $\min_{l\neq j} \Delta q_{j,l}$ represents the smallest Euclidean distance attainable between the fingerprint vector of atom j and some other atomic fingerprint vector of atom l.

The entropy term is then used to modify the total energy such that it becomes $E_{total} = E_{DFT} + KS(\{\mathbf{q}\})$ where K is an adjustable parameter used to control the effect of fingerprint entropy on the final structure, and DFT refers to density functional theory. When K is positive, structures will tend towards dis-similar local environments for each atom which leads to a more efficient training dataset. A total of 1,250 structures are initialized in a $2 \times 2 \times 1$ supercell of the conventional unit cell for the rocksalt configuration of CdSe and 500 structures are initialized in a $2 \times 2 \times 2$ supercell of the wurtzite structure, which yields 16 Cd and 16 Se atoms for all structures. Velocities for each atom are then chosen from a Maxwell-Boltzmann distribution for a temperature of 10,000 K and annealed down to 0 K with a timestep of 2.5 femtoseconds over a time period of 0.75 picoseconds. Simultaneously, the K term in the calculation for total energy is raised from 0 at 10,000 K to 100 at 0 K. This allows structures to relax into random but maximally disordered configurations. Forces are calculated by using Heynman-Fellman forces from DFT plus the entropy-generated forces which are simply derivatives with respect to atomic positions of the entropy term.

An additional 500 structures are generated using the same technique, but with K going from 0 to 100. This promotes highly symmetric structures, allowing the neural network to describe these types of configurations more accurately. Furthermore, we performed MD simulations with both the rocksalt and wurtzite structures to generate an additional 2,000 training points. An isothermal-isochoric (NVT) ensemble with an Andersen thermostat was used to maintain a temperature of 5,000 K with a timestep of 2.5 femtoseconds over a time period of 2.5 picoseconds. The MD simulations added structures that could be naturally attained by the CdSe system rather than being artificially created by maximizing or minimizing entropy.

A total of 4,250 training structures were generated which were then filtered for structures with a DFT energy below 0 eV and a maximum force of 100 eV/Å. This filtering yields 3,753 structures which are then split into 2,700 training structures, 302 validation structures and 751 structures reserved for testing.

DFT calculations

Energy and force calculations for the training dataset were performed using DFT within the Vienna ab initio simulation package (VASP)[56]. The projector augmented wave (PAW) method was employed to describe the electron-ion interactions[57]. The Perdew-Burke-Ernzerhof revised for solids (PBEsol) functional[58,59] was used to model the electron-electron interactions. A plane-wave basis set with a kinetic energy cutoff of 400 eV was utilized to expand the electronic wavefunctions. Monkhorst-Pack k-point meshes[60] with a grid of spacing $0.03\times2\pi$Å^{-1} for Brillouin zone sampling were chosen after checking for convergence. The convergence criteria for the electronic self-consistent field calculation were set to 10^{-6} eV. The total energy and atomic forces were calculated for each structure in the training dataset, providing the reference values for training the ML potential.

NequIP model training

With the dataset in place, we proceeded to train the NequIP model. The process involved the following key steps:

1. Data Preprocessing: Atomic numbers are first one-hot encoded into feature vectors of length 48, which are built from direct sums of the irreducible representations of the O(3) symmetry group.
2. Model Architecture: The one-hot encoded feature vector is then refined through four interaction blocks, which encode interactions between atoms in the unit cell and neighbors within the cutoff radius of 5 Å through a convolution filter. The convolution filter involves a tensor product with a learnable radial function and spherical harmonics. Since the convolution filters involve tensor products with spherical harmonic functions, a maximum rotation order is set to $l_{max} = 2$. Tensor products that produce irreducible representations with $l > l_{max}$ are discarded. The learnable radial functions are implemented as a multi-layer perceptron with two radial layers, each containing 64 neurons with SiLU activation functions. Eight basis functions were used in the basis embedding of the interatomic distances. Finally, the $l = 0$ features of the final convolution layer are passed to two atom-wise self-interaction layers which produce each atom's contribution to the total energy. Forces can be computed by taking the derivative with respect to atomic positions.
3. Training Process: We used the Adam optimizer with an initial learning rate of 5×10^{-3} and a batch size of 5. The learning rate was reduced by a factor of 0.5 every 100 epochs if no improvement in validation loss was observed. Training continued until convergence, which was defined as when error of the validation dataset reached below 2 meV/atom. One model was trained on energies and forces, with another being trained purely on stresses.

Integration with PALLAS

The trained NequIP model was the foundation for investigating the phase transition pathways of CdSe using the PALLAS method. By providing a fast and accurate approach for calculating the energies and forces of various atomic configurations encountered during the transition, the NequIP model enabled efficient exploration of the PES. To achieve seamless integration, a custom interface was developed to connect the NequIP model with the PALLAS method. This synergy allowed rapid evaluation of the energies and forces for intermediate structures along potential pathways, offering a computationally efficient means of exploring the energy landscape. The high accuracy of the NequIP model ensured precise identification and characterization of transition states and metastable intermediates, uncovering novel transition mechanisms that might have been overlooked by traditional methods. The computational efficiency of NequIP, combined with the systematic pathway exploration of PALLAS, enabled us to investigate regions of the PES that would be prohibitively expensive using *ab initio* methods alone.

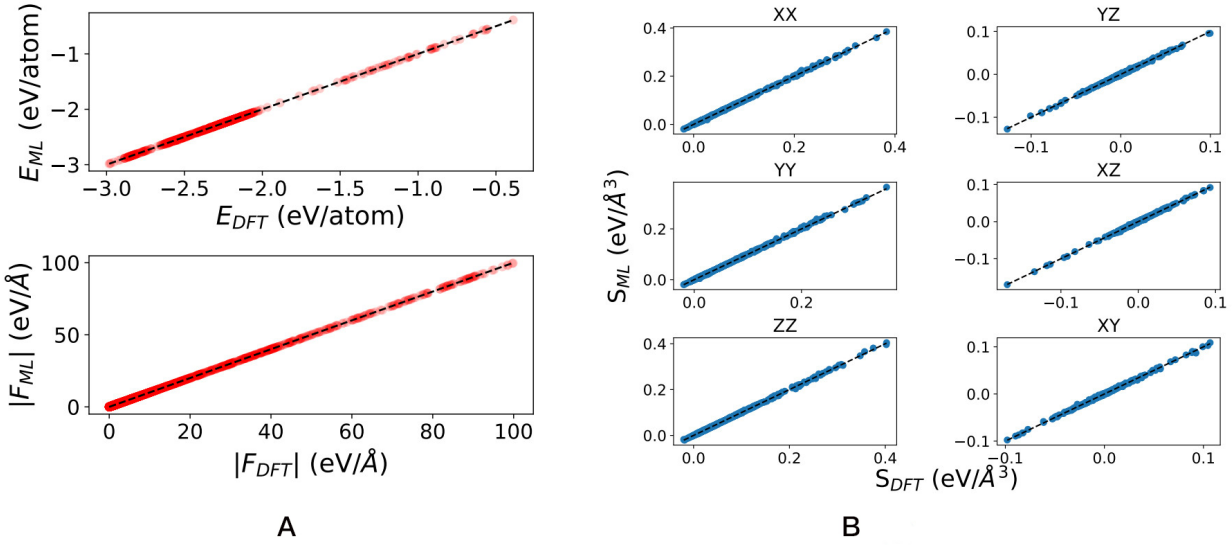

Figure 1. Graph of comparison of neural network predictions for (A) energies and forces and (B) stress versus the DFT calculated energies, forces and stresses for the 751 structures in the testing set. The black dashed line represents perfect agreement between the prediction by the neural network and the DFT calculated value. MAEs of the energies and the forces were 1.8 meV/atom and 33 meV/Å, respectively. The stress plot shows predictions versus DFT values for each Voigt component of the stress, with average errors for every component below 10^{-5} eV/Å^3. DFT: Density functional theory; MAEs: mean absolute errors.

RESULTS AND DISCUSSION

Validation of machine learning potential

Building on the detailed methodology involving the use of machine-learned interatomic potentials, we proceeded to validate the accuracy and reliability of our ML potential for CdSe. The validation was conducted through the analysis of 751 diverse configurations, representing a broad spectrum of the material phase space. This subset, spanning a large energy range (-3.0 to -0.5 eV/atom), was instrumental in evaluating the robustness of the model across different structural motifs of CdSe. The evaluation included a comparative analysis of the energies and atomic forces predicted by our ML model against those derived from DFT calculations [Figure 1]. Specifically, we observed mean absolute errors (MAEs) in energy predictions to be minimal, closely aligning with DFT benchmarks, thereby indicating a high level of accuracy in the energy landscape representation. Similarly, the atomic forces predicted by the model demonstrated a strong correlation with DFT-calculated forces, underscoring the precision of our model in capturing dynamic interactions within the CdSe system.

Further validation was conducted through the analysis of several key structures, including the wurtzite, rocksalt, and zinc blende phases of CdSe. The total energy differences between DFT and the ML potential were 12, 5, and 16 meV/atom, respectively. Validation was also performed on several transition states predicted by the PALLAS method, with total energy differences between DFT and the ML potential being 9 meV/atom. This comprehensive validation process affirmed the capability of the NequIP-trained ML potential in accurately modeling the PES of CdSe and highlighted its potential in facilitating advanced studies of material properties and phase transitions.

Phase transition pathway network in CdSe

The application of the PALLAS method to the wurtzite to rocksalt phase transition in CdSe revealed a complex network of transition pathways, as illustrated in Figure 2. This network provides a comprehensive view of the potential energy landscape connecting the wurtzite and rocksalt phases of CdSe. The transition pathway network spans an energy range of approximately 1.6 eV/atom, with the wurtzite and rocksalt structures positioned at the lower energy regions of the network. This energy spread indicates the presence of numerous metastable

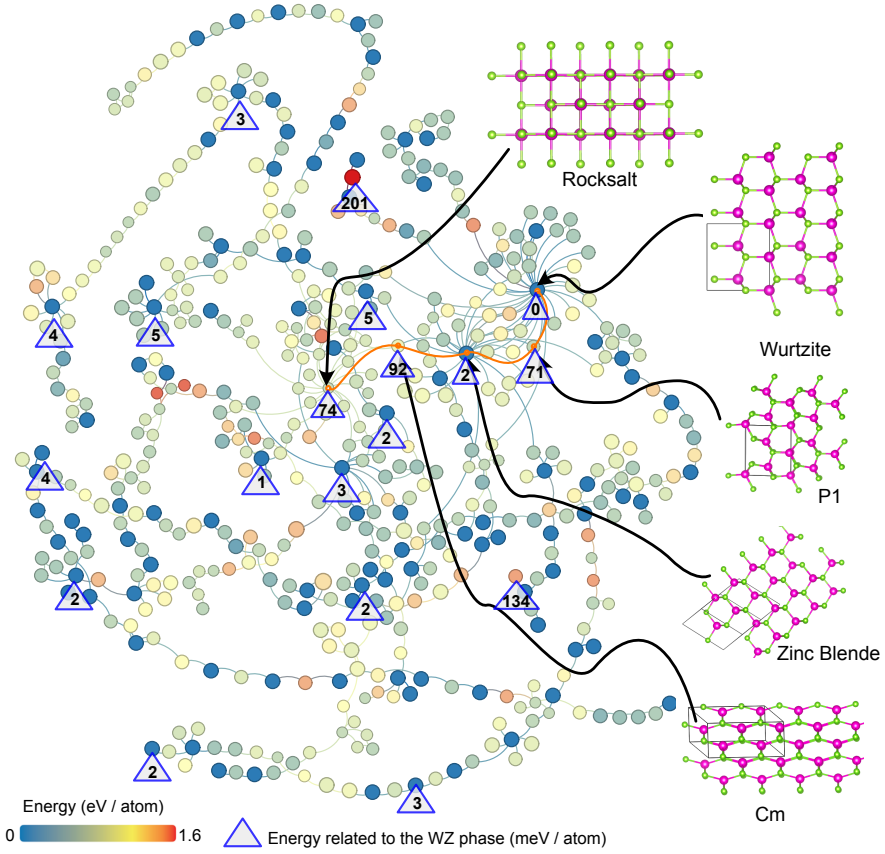

Figure 2. Transition pathway network for the wurtzite to rocksalt transformation in CdSe. Nodes represent distinct structural configurations, while edges indicate transition pathways. The color gradient from blue to red represents increasing energy, with energy values given in eV/atom relative to the wurtzite structure. Blue triangles indicate the energy differences (in meV/atom) between the corresponding nodes and the wurtzite phase. Many metastable structures are observed, with several nodes exhibiting energies close to that of the wurtzite phase; however, none are lower in energy than wurtzite. These nodes correspond to metastable structures that may become accessible during the phase transition under certain external conditions (e.g., pressure or temperature). The orange line represents the lowest-energy pathway connecting the wurtzite and rocksalt structures.

intermediate states and transition pathways connecting the two phases. The network topology reveals several key features. The existence of numerous interconnected nodes between the wurtzite and rocksalt structures suggests multiple possible transition mechanisms, each with varying energy barriers. Several nodes in the mid-energy range of the network likely represent metastable intermediate structures, which could play crucial roles in the transformation process, potentially serving as kinetic traps or facilitating the overall transition.

The transition pathway network allows for the identification of the lowest energy pathway connecting the wurtzite and rocksalt phases. This optimal path, highlighted in orange in Figure 2, represents the most thermodynamically favorable transition mechanism. The colors of nodes in the network provide insight into the energy barriers associated with different transition steps. Higher-energy nodes along a pathway indicate significant barriers that may kinetically hinder the transformation. Furthermore, the network structure provides information about potential kinetic bottlenecks and metastable states that could influence the transformation dynamics. Intermediate nodes in the network represent predicted metastable structures of CdSe, some of which may be experimentally accessible and exhibit interesting properties. The identified pathways and intermediate states may offer guidance for experimental efforts aimed at controlling the phase transition process and potentially accessing novel metastable forms of CdSe.

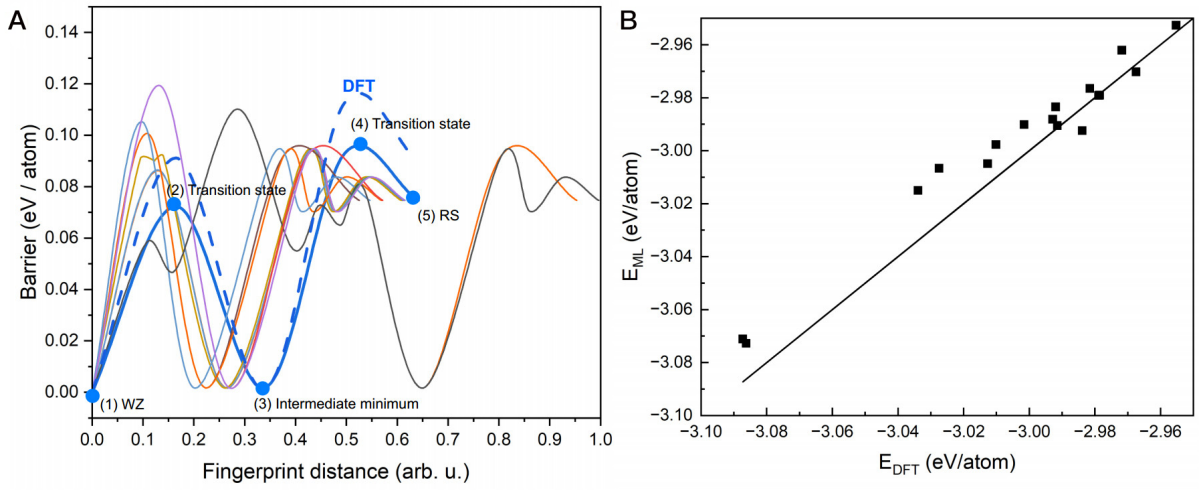

Figure 3. (A) Energy barriers of transition pathways extracted from the pathway network. The lowest energy pathway is highlighted with a thick blue line. The dashed blue line represents the barrier calculated using DFT for the lowest-energy pathway; (B) Graph of comparison of neural network predictions for energies the DFT calculated energies for the crucial points along the transition pathway, including metastable states and transition states depicted in (A). MAE of the energies was 9 meV/atom. DFT: Density functional theory; MAE: mean absolute error.

Microscopic mechanism of CdSe phase transitions

The PALLAS method has provided valuable insights into the microscopic mechanisms of the wurtzite to rocksalt phase transition in CdSe. Figure 3A illustrates the energy profile of several transition pathways, with the lowest energy pathway highlighted by a thick blue line. Figure 3B further validates the accuracy of the machine-learned potential by comparing the predicted energies along the transition pathway to DFT-calculated values. The close agreement, with a MAE of only 9 meV/atom, highlights the reliability of the PALLAS+NequIP framework in capturing the intricate details of the PES. The energetic landscape, coupled with the structural configurations along the pathway shown in Figure 4, offers a comprehensive view of the transformation process.

The lowest energy pathway reveals a complex, multi-step transformation that challenges the notion of a simple, direct transition between the wurtzite and rocksalt phases. Beginning with the hexagonal wurtzite structure ($P6_3mc$ space group), the system first evolves through a transition state with $P1$ symmetry. This low symmetry configuration suggests a distortion of the wurtzite lattice, likely involving a shear deformation that breaks the initial hexagonal symmetry. Intriguingly, the pathway then passes through a stable intermediate minimum with $F\bar{4}3m$ symmetry. This face-centered cubic structure, recognized as the zinc blende phase, plays a pivotal role in the transition process. Its presence indicates that the wurtzite to rocksalt transformation in CdSe can involve a metastable intermediate phase, rather than proceeding directly.

An interesting feature of our PALLAS simulations is the prevalence of the zinc blende intermediate across the majority of identified transition pathways. This consistent appearance suggests that the zinc blende structure serves as a crucial facilitator in the wurtzite to rocksalt transformation, potentially providing a lower energy kinetic pathway between the hexagonal and cubic phases. The importance of the zinc blende phase in our computational results aligns with experimental observations in the literature. For example, wurtzite/zinc blende mixed phase CdSe structures have been reported in various studies, indicating the coexistence of these two phases under certain conditions[18,61]. Studies also demonstrated controlled synthesis of CdSe nanocrystals in both wurtzite and zinc blende phases through careful selection of ligands and reaction temperatures[61].

Following the zinc blende intermediate, the system traverses a second transition state with Cm symmetry. The

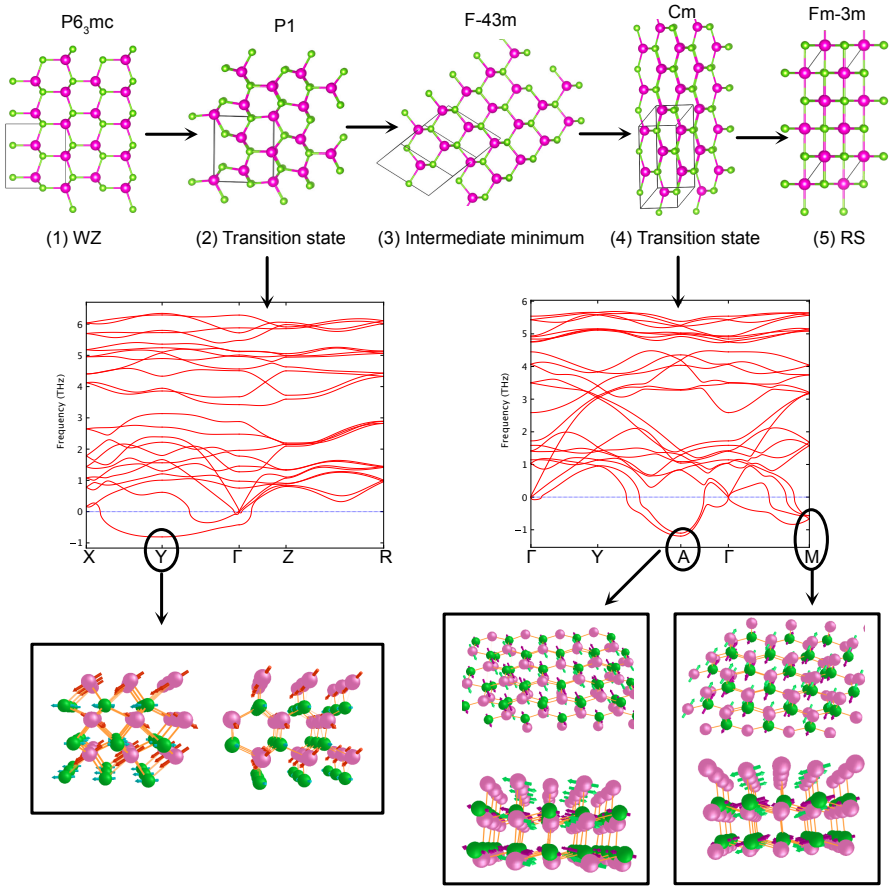

Figure 4. (Upper panel) Structural configurations along the lowest-energy transition pathway from wurtzite (WZ) to rocksalt (RS) in CdSe. Red and green spheres represent Cd and Se atoms, respectively. (Middle panel) Calculated phonon dispersion curves for the transition states of CdSe. (Lower panel) Arrows indicate the eigenvectors of the softened phonon modes at the Y point of the P1 structure and at the A and M points of the Cm structure.

low symmetry in this configuration points to a complex atomic rearrangement, likely involving significant distortions of the crystal lattice. Finally, the system reaches the highly symmetric rocksalt structure ($Fm\bar{3}m$ space group), completing the phase transition. The contrast between the *Cm* transition state and the final rocksalt structure suggests a sudden symmetrization in the final stage of the transformation. This two-stage transformation mechanism is consistent with the previous study performed using NEB calculations[28].

To further elucidate the dynamical properties of the key transition states along the pathway, we conducted phonon calculations for the two transition states using the Phonopy code[62]. For the $P1$ structure, the phonon dispersion curve reveals the most softened phonon mode at the Y point [Figure 4]. The corresponding eigenvector indicates a shear motion of Cd and Se atoms, consistent with the lattice distortions expected during the transition from wurtzite to the zinc blende intermediate. Similarly, for the *Cm* structure, phonon dispersion reveals softened modes at the A and M points. The eigenvectors of these modes suggest concerted atomic displacements, likely corresponding to compressive and shear strains that drive the transformation toward the rocksalt phase. The presence of these soft modes emphasizes the importance of lattice instabilities in enabling the multi-step transition pathway.

Our study provides a detailed characterization of the phase transition pathways in CdSe, focusing on the transformation from the wurtzite to rocksalt phase. While it is well-established that the wurtzite structure represents

the ground state and that the zinc blende phase is a close metastable structure, our findings introduce new insights into the transition mechanism. Specifically, we identify zinc blende as an intermediate structure along the wurtzite-to-rocksalt transition pathway. This theoretical prediction highlights a previously unrecognized role of zinc blende in facilitating the transition by providing a lower-energy kinetic pathway between the two phases.

The zinc blende intermediate might be stabilized under certain conditions, potentially allowing for the isolation of this metastable phase or the creation of mixed-phase CdSe with tunable properties. The importance of the zinc blende structure in the transition pathways may also help explain the often-observed coexistence of wurtzite and zinc blende phases in CdSe nanostructures[18,61]. Our simulations suggest that nanoscale CdSe might readily fluctuate between these two structures. The transition through the zinc structure could be a mechanism for stacking fault formation in CdSe, as incomplete transitions could result in mixed wurtzite/zinc blende regions. Controlled synthesis methods, such as chemical vapor deposition[63] or solution-phase synthesis[64], may enable the formation of the zinc blende phase as a metastable state. Furthermore, transient detection of the zinc blende intermediate during phase transitions may be possible using advanced characterization techniques. For example, time-resolved spectroscopy could track structural changes dynamically, while in situ high-pressure X-ray diffraction experiments might reveal intermediate phases under appropriate thermodynamic conditions[65,66]. These approaches provide promising avenues for validating our findings experimentally and for exploring the broader relevance of the zinc blende intermediate in phase transition mechanisms.

It is worth noting that our study focused on the phase transition at ambient pressure and low temperatures. At finite temperatures, the free energy landscape may differ significantly from the zero-temperature potential energy landscape. Entropic contributions can stabilize or destabilize certain metastable states, potentially altering the transition pathways or introducing new mechanisms. Future extensions of this framework could incorporate free energy calculations to account for temperature effects. Techniques such as thermodynamic integration[67], or enhanced sampling methods (e.g., metadynamics[68,69]) could be used to compute the finite-temperature free energy landscape. These methods would allow for a more comprehensive understanding of phase transitions, including how temperature-dependent effects influence the stability of metastable states and the dynamics of the transformation process.

CONCLUSIONS

This study has demonstrated the power of combining ML potentials with swarm intelligence-based pathway sampling methods to elucidate the complex phase transition mechanisms in CdSe. By integrating the NequIP ML potential with the PALLAS method, we have achieved a detailed understanding of the wurtzite to rocksalt phase transition at an unprecedented level of accuracy and computational efficiency. Our ML potential showed excellent agreement with DFT calculations, ensuring reliable exploration of the CdSe PES. The PALLAS method revealed a complex network of transition pathways between the wurtzite and rocksalt phases, highlighting the intricate nature of the phase transition landscape in CdSe. A key finding of our work is the identification of a novel, multi-step transition mechanism involving an unexpected zinc blende intermediate phase. This zinc blende structure appears to play a crucial role in facilitating the transition between wurtzite and rocksalt phases. The prevalence of the zinc blende intermediate across multiple pathways suggests its importance in the structural flexibility of CdSe, aligning with experimental observations of wurtzite/zinc blende coexistence in CdSe nanostructures and offering an explanation for the formation of stacking faults. Our results provide new insights into the energetics and kinetics of the phase transition, identifying key transition states and energy barriers that could be targeted for controlling the transformation process.

These findings have implications for both fundamental materials science and practical applications of CdSe.

The detailed transition pathway network provides a roadmap for experimental efforts aimed at controlling phase transitions in CdSe, potentially enabling the synthesis of novel metastable forms or mixed-phase materials with tailored properties. Our methodology demonstrates the potential for ML-enhanced computational techniques to accelerate materials discovery and optimization, particularly in systems with complex phase behavior. The synergy between ML potentials and swarm intelligence-based pathway sampling opens new avenues for materials design and discovery. Future work could focus on experimental validation of the predicted transition mechanisms, exploration of pressure and size-dependent effects on the transition pathways, and extension of this methodology to other technologically relevant materials systems.

DECLARATIONS

Authors' contributions

Conceptualization, resources, supervision, calculation, writing, review, and editing: Zhu L
Simulation, data curation, writing: Wang M
Simulation, data curation, machine learning potential training, writing: Rao R

Availability of data and materials

The data and source code that support the findings of this study are available from the corresponding author upon reasonable request.

Financial support and sponsorship

This work was supported by the National Science Foundation, Division of Materials Research (NSF-DMR) under Grant No. 2226700 and startup funds of the Office of the Dean of SASN of Rutgers University, Newark. The authors acknowledge the Office of Advanced Research Computing (OARC) at Rutgers, The State University of New Jersey, for providing access to the Amarel cluster and associated research computing resources that have contributed to the results reported here.

Conflicts of interest

All authors declared that there are no conflicts of interest.

Ethical approval and consent to participate

Not applicable.

Consent for publication

Not applicable.

REFERENCES

1. Ninomiya S, Adachi S. Optical properties of cbic and hexagonal CdSe. *J Appl Phys* 1995;78:4681–89. DOI
2. Park SH, Casey MP, Falk J. Nonlinear optical properties of CdSe quantum dots. *J Appl Phys* 1993;73:8041–45. DOI
3. Yuan J, Chen Y, Duan X, Yao B, Dai T, et al. CdSe optical parametric oscillator operating at 12.07 μm with 170 mW output. *Opt Laser Technol* 2017;92:1–4. DOI
4. Wu K, Lian T. Quantum confined colloidal nanorod heterostructures for solar-to-fuel conversion. *Chem Soc Rev* 2016;45:3781–810. DOI
5. Du Z, Artemyev M, Wang J, Tang J. Performance improvement strategies for quantum dot-sensitized solar cells: a review. *J Mater Chem A* 2019 Feb;7:2464–89. DOI
6. Schierhorn M, Boettcher SW, Kraemer S, Stucky GD, Moskovits M. Photoelectrochemical performance of CdSe nanorod arrays grown on a transparent conducting substrate. *Nano Lett* 2009;9:3262–7. DOI
7. Liu M, Chen ZY, He XH, et al. Thermodynamics of ligand exchange with aromatic ligands on the surface of CdSe quantum dots. *Chem Mater* 2023;35:1868–76. DOI

8. Protesescu L, Nachtegaal M, Voznyy O, et al. Atomistic description of thiostannate-capped CdSe nanocrystals: retention of four-coordinate SnS4 motif and preservation of Cd-rich stoichiometry. *J Am Chem Soc* 2015;137:1862–74. DOI
9. Pan D, Wang Q, Pang J, Jiang S, Ji X, An L. Semiconductor "nano-onions" with multifold alternating CdS/CdSe or CdSe/CdS structure. *Chem Mater* 2006;18:4253–8. DOI
10. Soni U, Pal A, Singh S, et al. Simultaneous type-I/type-II emission from CdSe/CdS/ZnSe nano-heterostructures. *ACS Nano* 2014;8:113–23. DOI
11. Grünwald M, Rabani E, Dellago C. Mechanisms of the wurtzite to rocksalt transformation in CdSe nanocrystals. *Phys Rev Lett* 2006;96:255701. DOI
12. Benkhettou N, Rached D, Soudini B, Driz M. High-pressure stability and structural properties of CdS and CdSe. *Phys Status Solidi B* 2004;241:101–7. DOI
13. Zahn D, Grin Y, Leoni S. Mechanism of the pressure-induced wurtzite to rocksalt transition of CdSe. *Phys Rev B* 2005;72:064110. DOI
14. Bealing C, Martoňák R, Molteni C. Pressure-induced structural phase transitions in CdSe: a metadynamics study. *J Chem Phys* 2009;130:124712. DOI
15. Bealing C, Martoňák R, Molteni C. The wurtzite to rock salt transition in CdSe: a comparison between molecular dynamics and metadynamics simulations. *Solid State Sci* 2010;12:157–62. DOI
16. Durandurdu M. Orthorhombic intermediate phases for the wurtzite-to-rocksalt phase transformation of CdSe: an ab initio constant pressure study. *Chem Phys* 2010;369:55–8. DOI
17. Shimojo F, Kodiyalam S, Ebbsjö I, Kalia RK, Nakano A, Vashishta P. Atomistic mechanisms for wurtzite-to-rocksalt structural transformation in cadmium selenide under pressure. *Phys Rev B* 2004;70:184111. DOI
18. Tolbert SH, Alivisatos AP. The wurtzite to rock salt structural transformation in CdSe nanocrystals under high pressure. *J Chem Phys* 1995;102:4642–56. DOI
19. Stokes HT, Gunter J, Hatch DM, Dong J, Wang H, Lewis JP. Bilayer sliding mechanism for the wurtzite-to-rocksalt transition. *Phys Rev B* 2007;76:012102. DOI
20. Fan H, Liang J, Zhang Y, et al. Phase transition of CdSe nanocrystallines with controlled morphologies induced by ratios of ethanolamine and water in their mixed solution. *Solid State Sci* 2008;10:901–7. DOI
21. Li Y, Lin C, Li G, Xu J, Li X, Liu J. Structure determination of the high-pressure phase of CdSe. *J Appl Phys* 2014;115:223507. DOI
22. Tolbert SH, Alivisatos AP. Size dependence of a first order solid-solid phase transition: the wurtzite to rock salt transformation in CdSe nanocrystals. *Science* 1994;265:373–6. DOI
23. Li B, Bian K, Zhou X, et al. Pressure compression of CdSe nanoparticles into luminescent nanowires. *Sci Adv* 2017;3:e1602916. DOI
24. Ibrahimova LN, Abdullayev NM, Aliyev ME, Garashova GA, Aliyev YI. Phase formation process in CdSe thin films. *East Eur J Phys* 2024;493–6. DOI
25. Dhara S, Liu CP, Chen SF, Eliseev AA, Petukhov DI. Resonance raman spectroscopic study of shape-induced phase transition in CdSe nanoclusters. *J Raman Spectrosc* 2015;46:1–3. DOI
26. Rivera-Marquez JA, Contreras-Rascón JI, Lozada-Morales R, et al. Raman spectroscopy study of the wurtzite-zinc blende phase transition of bare CdSe nanoparticles. *Mater Sci Eng B* 2020;260:114621. DOI
27. Zhang L, Yang M, Zhang S, Niu H. Unveiling the crystallization mechanism of cadmium selenide via molecular dynamics simulation with machine-learning-based deep potential. *J Mater Sci Technol* 2024;185:23–31. DOI
28. Sheppard D, Xiao P, Chemelewski W, Johnson DD, Henkelman G. A generalized solid-state nudged elastic band method. *J Chem Phys* 2012;136:074103. DOI
29. Qian GR, Dong X, Zhou XF, Tian Y, Oganov AR, et al. Variable cell nudged elastic band method for studying solid-solid structural phase transitions. *Comput Phys Commun* 2013;184:2111–8. DOI
30. Dellago C, Bolhuis PG, Chandler D. Efficient transition path sampling: application to Lennard-Jones cluster rearrangements. *J Chem Phys* 1998;108:9236–45. DOI
31. Bolhuis PG, Chandler D, Dellago C, Geissler PL. Transiton path sampling: throwing ropes over rough mountain passes, in the dark. *Ann Rev Phys Chem* 2002;53:291–318. DOI
32. Zhu L, Cohen RE, Strobel TA. Phase transition pathway sampling via swarm intelligence and graph theory. *J Phys Chem Lett* 2019;10:5019–26. DOI
33. Eberhart RC, Shi Y. Comparing inertia weights and constriction factors in particle swarm optimization. In: Proceedings of the 2000 Congress on Evolutionary Computation. CEC00 (Cat. No.00TH8512); 2000 Jul 16-19; La Jolla, USA. IEEE; 2000. pp. 84–8. DOI
34. Dorigo M, Birattari M, Stutzle T. Ant colony optimization. *IEEE Comput Intell Mag* 2006;1:28–39. DOI
35. Behler J. Perspective: machine learning potentials for atomistic simulations. *J Chem Phys* 2016;145:170901. DOI
36. Braeckevelt T, Goeminne R, Vandenhaute S, et al. Accurately determining the phase transition temperature of $CsPbI_3$ via random-phase approximation calculations and phase-transferable machine learning potentials. *Chem Mater* 2022;34:8561–76. DOI
37. Verdi C, Karsai F, Liu P, Jinnouchi R, Kresse G. Thermal transport and phase transitions of zirconia by on-the-fly machine-learned interatomic potentials. *npj Comput Mater* 2021;7:156. DOI
38. Wisesa P, Andolina CM, Saidi WA. Machine-learning accelerated first-principles accurate modeling of the solid-liquid phase transition in MgO under mantle conditions. *J Phys Chem Lett* 2023;14:8741–8. DOI
39. Zhao Y, Sun J, Yang L, Zhai D, Sun L, Deng W. Umbrella sampling with machine learning potentials applied for solid phase transition of GeSbTe. *Chem Phys Lett* 2022;803:139813. DOI
40. Fantasia A, Rovaris F, Abou El Kheir O, et al. Development of a machine learning interatomic potential for exploring pressure-dependent

kinetics of phase transitions in germanium. *J Chem Phys* 2024;161:014110. DOI
41. Santos-Florez PA, Yanxon H, Kang B, Yao Y, Zhu Q. Size-dependent nucleation in crystal phase transition from machine learning metadynamics. *Phys Rev Lett* 2022;129:185701. DOI
42. Rabani E. An interatomic pair potential for cadmium selenide. *J Chem Phys* 2002;116:258-62. DOI
43. Xiao P, Sheppard D, Rogal J, Henkelman G. Solid-state dimer method for calculating solid-solid phase transitions. *J Chem Phys* 2014;140:174104. DOI
44. Zhu L, Amsler M, Fuhrer T, et al. A fingerprint based metric for measuring similarities of crystalline structures. *J Chem Phys* 2016;144:034203. DOI
45. Coello CAC, Pulido GT, Lechuga MS. Handling multiple objectives with particle swarm optimization. *IEEE Trans Evol Comput* 2004;8:256–79. DOI
46. Even S. Graph algorithms. 2nd edition. Cambridge University Press; 2011. DOI
47. Sadeghi A, Ghasemi SA, Schaefer B, Mohr S, Lill MA, Goedecker S. Metrics for measuring distances in configuration spaces. *J Chem Phys* 2013;139:184118. DOI
48. Parsaeifard B, Sankar De D, Christensen AS, et al. An assessment of the structural resolution of various fingerprints commonly used in machine learning. *Mach Learn Sci Technol* 2021;2:015018. DOI
49. Parsaeifard B, De DS, Finkler JA, Goedecker S. Fingerprint-based detection of non-local effects in the electronic structure of a simple single component covalent system. *Condens Matter* 2021;6:9. DOI
50. Parsaeifard B, Goedecker S. Manifolds of quasi-constant SOAP and ACSF fingerprints and the resulting failure to machine learn four-body interactions. *J Chem Phys* 2022;156:034302. DOI
51. Tao S, Shao X, Zhu L. Accelerating structural optimization through fingerprinting space integration on the potential energy surface. *J Phys Chem Lett* 2024;15:3185–90. DOI
52. Kruskal JB, Jr. On the shortest spanning subtree of a graph and the traveling salesman problem. *Proc Am Math Soc* 1956;7:48–50. Available from: http://5010.mathed.usu.edu/Fall2018/THigham/Krukskal.pdf [Last accessed on 21 Dec 2024]
53. Moore EF. The shortest path through a maze. In: Proceedings of the International Symposium on the Theory of Switching. 1959. pp. 285–92. Available from: https://scirp.org/reference/referencespapers?referenceid=3304833 [Last accessed on 21 Dec 2024]
54. Batzner S, Musaelian A, Sun L, et al. E(3)-equivariant graph neural networks for data-efficient and accurate interatomic potentials. *Nat Commun* 2022;13:2453. DOI
55. Martinez B JA, Shao X, Jiang K, Pavanello M. Entropy is a good approximation to the electronic (static) correlation energy. *J Chem Phy* 2023;159:191102. DOI
56. Kresse G, Furthmüller J. Efficient iterative schemes for *ab initio* total-energy calculations using a plane-wave basis set. *Phys Rev B* 1996;54:11169. DOI
57. Blöchl PE. Projector augmented-wave method. *Phys Rev B* 1994;50:17953. DOI
58. Perdew JP, Burke K, Ernzerhof M. Generalized gradient approximation made simple. *Phys Rev Lett* 1996;77:3865. DOI
59. Perdew JP, Ruzsinszky A, Csonka GI, et al. Restoring the density-gradient expansion for exchange in solids and surfaces. *Phys Rev Lett* 2008;100:136406. DOI
60. Monkhorst HJ, Pack JD. Special points for Brillouin-zone Integrations. *Phys Rev B* 1976;13:5188. DOI
61. Huang J, Kovalenko MV, Talapin DV. Alkyl chains of surface ligands affect polytypism of CdSe nanocrystals and play an important role in the synthesis of anisotropic nanoheterostructures. *J Am Chem Soc* 2010;132:15866–8. DOI
62. Togo A. First-principles phonon calculations with phonopy and phono3py. *J Phys Soc Jpn* 2023;92:012001. DOI
63. Meng Y, Yan C, Lai J, et al. Enhanced optical properties of chemical vapor deposited single crystal diamond by low-pressure/high-temperature annealing. *Proc Natl Acad Sci U S A* 2008;105:17620–5. DOI
64. Cargnello M, Gordon TR, Murray CB. Solution-phase synthesis of titanium dioxide nanoparticles and nanocrystals. *Chem Rev* 2014;114:9319–45. DOI
65. Greetham GM, Burgos P, Cao Q, Clark IP, Codd PS, et al. Ultra: a unique instrument for time-resolved spectroscopy. *Appl Spectrosc* 2010;64:1311–9. Available from: https://www.researchgate.net/publication/49670159_Ultra_A_Unique_Instrument_for_Time-Resolved_Spectroscopy [Last accessed on 21 Dec 2024]
66. Robert E, Khacef A, Cachoncinlle C, Pouvesle JM. Time-resolved spectroscopy of high pressure rare gases excited by an energetic flash X-ray source. *Opt Commun* 1995;117:179–88. DOI
67. Alfè D, Price GD, Gillan MJ. Thermodynamics of hexagonal-close-packed iron under Earth's core conditions. *Phys Rev B* 2001;64:045123. DOI
68. Micheletti C, Laio A, Parrinello M. Reconstructing the density of states by history-dependent metadynamics. *Phys Rev Lett* 2004;92:170601. DOI
69. Barducci A, Bussi G, Parrinello M. Well-tempered metadynamics: a smoothly converging and tunable free-energy method. *Phys Rev Lett* 2008;100:020603. DOI